Exciting Cell Membranes with a Blustering Heat Shock

Qiang Liu,[†] Micah J. Frerck,[‡] Holly A. Holman,[‡] Erik M. Jorgensen,[†§] and Richard D. Rabbitt[‡¶*]
[†]Department of Biology, [‡]Department of Bioengineering, and [§]Howard Hughes Medical Institute, University of Utah, Salt Lake City, Utah; and [¶]Marine Biological Laboratory, Woods Hole, Massachusetts

ABSTRACT Brief heat shocks delivered to cells by pulsed laser light can evoke action potentials in neurons and contraction in cardiomyocytes, but the primary biophysical mechanism has been elusive. In this report we show in the neuromuscular junction of *Caenorhabditis elegans* that application of a 500°C/s heat shock for 500 μs evoked ~35 pA of excitatory current and injected ~23 fC(femtocoulomb) of charge into the cell while raising the temperature only 0.25°C. The key variable driving the current was the rate of change of temperature (*dT*/*dt* heat shock), not temperature itself. The photothermal heat shock current was voltage-dependent and was from thermally driven displacement of ions near the plasma membrane. The charge movement was rapid during the heat shock and slow during thermal relaxation, thus leading to an asymmetrical capacitive current that briefly depolarized the cell. A simple quantitative model is introduced to describe modulation of the membrane potential and facilitate practical application of optical heat shock stimuli.

INTRODUCTION

Transient heat pulses, delivered to cells by absorption of infrared (IR) light by water, have been shown to modulate intracellular signaling (1,2), trigger action potential generation and neurotransmitter release in neurons (3–7), and evoke contraction in cardiomyocytes (2,8,9). Cells are sensitive to the magnitude of temperature change (ΔT) delivered by each pulse as well as the time rate of change of temperature during the pulse, or heat shock (dT/dt) (10,11). Sensitivity reported in the literature, however, is highly variable due to diversity in the endogenous expression of temperature-sensitive ion channels and molecular signaling cascades, and differences in optical stimulus parameters used between different studies (12–16).

This diversity has led to considerable debate about the practical usefulness of photothermal stimuli and begs the question whether any universal excitatory photothermal mechanisms exist. It was recently demonstrated in model membranes and cell lines that optically delivered heat shocks evoke transient capacitive currents across the cell membrane that are present even in the complete absence of ion channels (17). These heat-shock-evoked electrical currents are in fact predicted by classical models of the electrochemical double-layer adjacent to the cell membrane (18–20). Rapidly increasing the temperature increases molecular diffusion within the electrical double layer and drives net ionic charge away from the plasma membrane. The charge movement differs on the intracellular versus extracellular sides of the membrane, and thus leads to a transient depolarizing current.

Based on its biophysical origin, the capacitive photothermal effect should also be present in vivo. Here, we confirm this prediction and expand upon the characterization of capacitive photothermal membrane currents using voltage-clamp recordings of the neuromuscular junction (NMJ) of *Caenorhabditis elegans.* A simple mathematical model is introduced to quantify results and facilitate application of capacitive photothermal stimuli. Results demonstrate how optical heat pulses can be applied to perturb the whole-cell membrane potential and to transiently manipulate the ionic microenvironment near the membrane.

MATERIALS AND METHODS

Young adult hermaphrodite *C. elegans* were used as described previously in Liu et al. (21). Strains included: wild-type *C. elegans* Bristol (WT, N2), and:

CB407 *unc-49*(*e407*),
EG1584 *unc-38*(*e264*) *unc-49*(*e407*),
EG5918 *unc-49*(*e407*) *acr-16*(*ok789*),
RB1052 *trpa-1*(*ok999*),
MT1685 *unc-105*(*n490n786*),
MT1098 *unc-105*(*n506*),
JT6228 *egl-23*(*n601sa179*),
CB4461 *unc-110*(*e1913e2383*),
JT11020 *unc-58*(*e665e2820*),
MT3649 *sup-9*(*n1549*),
MT3366 *unc-93*(*e1500n234e1490*), and
LY101 *slo-2*(*nf101*).

All experiments were performed with the bath at room temperature using a single-electrode (borosilicate glass, $R_E \approx 5M\Omega$) voltage-clamp (EPC-10; HEKA Elektronik, Lambrecht/Pfalz, Germany) with capacitive compensation optimized at rest, and series resistance compensated 50%.

Pipette solution: KCl 120 mM, KOH 20 mM, $MgCl_2$ 4 mM, TES (N-Tris hydroxymethyl methyl-2-aminoethane-sulfonic acid) 5 mM, $CaCl_2$ 0.25 mM, EGTA 5 mM, Na_2ATP 4 mM, Sucrose 36 mM.
Extracellular solution (standard, A): NaCl 150 mM, KCl 5 mM, $CaCl_2$ 1 mM, $MgCl_2$ 1 mM, Sucrose 5 mM, HEPES 15 mM, Glucose 10 mM.
Pipette solution for ion-substitution experiments: CsCl 140 mM, TEA-Cl (Tetraethylammonium chloride) 5 mM, TES 5 mM, EGTA 5 mM, MgATP 4 mM.

Submitted August 29, 2013, and accepted for publication March 6, 2014.
*Correspondence: r.rabbitt@utah.edu
Editor: Leonid Brown.

0006-3495/14/04/1570/8 $2.00
http://dx.doi.org/10.1016/j.bpj.2014.03.008

Solution B (with 0 K^+ and 0 Ca^{2+}): NaCl 100 mM, TEA-Cl 40 mM, $CaCl^2$ 0 mM, $MgCl^2$ 1 mM, 4-AP 3 mM, HEPES 10 mM, Glucose 20 mM.

Solution C (with 0 K^+ and 0 Na^+): Ca 5 mM, TEA-Cl 140 mM, $CaCl_2$ 5 mM, $MgCl_2$ 1 mM, 4-AP 3 mM, HEPES 10 mM, Glucose 20 mM.

Thermal stimuli were delivered via a cut and polished 400-μm-diameter low OH content optical fiber (VIS-NIR; Ocean Optics, Dunedin, FL), with the cut-end positioned ~400 μm from the cell. Unless otherwise noted, 1862-nm photothermal pulses were applied for 500 μs delivering ~1.5 mJ to the volume of water and tissue in front of the optical probe (Capella; Lockheed Martin, Bothel, WA). Energy output was measured in air ~400 μm in front of the cut end of the optical fiber (7Z02621; Ophir, Jerusalem, Israel), and temperature was measured in the fluid media ex situ by monitoring the impedance of a calibrated pulled glass pipette placed ~400 μm in front of the cut end of the optical fiber. Thermal stimuli were applied at 1–20 pulses per s (pps). Analog data were filtered at 2 kHz and digitized at 100 μs.

RESULTS

The rise in temperature during a 300–1500 μs IR pulse was linear, while relaxation to the prestimulus temperature was relatively slow and well approximated by a double-exponential

$$T = \Delta T\left\{\phi e^{-t/\tau_1} + (1-\phi)e^{-t/\tau_2}\right\},$$

where $\tau_1 = 0.65$, $\tau_2 = 0.084$, and $\phi = 0.454$, and ΔT is the single pulse temperature rise. Fig. 1 *a* shows the temperature rise generated in media by a single IR optical pulse (average, $n = 38$) determined by measuring the impedance change of a calibrated glass pipette (*inset*, example impedance change for one pulse). The temperature increased linearly in time during the IR pulse because the laser pulse was much shorter than the thermal relaxation time (linearity confirmed for IR pulses up to 3 ms, $R^2 > 0.99$; $n = 5$) (11). We define the heat shock stimulus as the time rate of change of temperature dT/dt, which was a constant ~500°C/s during the stimulus shown and became slightly negative during relaxation (Fig. 1 *b*, and see Norton and Bowler (11) for a more detailed analysis of the thermal transient). Consistent with previous reports in the NMJ, whole-cell voltage-clamp recordings at −60 mV revealed spontaneous miniature postsynaptic currents (mPSCs) associated with spontaneous presynaptic vesicle release (Fig. 1, *c–e*, inward transients, WT $n = 55$; whole-cell capacitance $C_m = 26 \pm 2.9$ pF; and series resistance $R_m = 25.0 \pm 11.2$ MΩ).

Three types of photothermal events were evoked by IR pulses:

1. The mPSC rate (Fig. 1 *c*) increased after each IR pulse, due to temperature sensitivity of presynaptic vesicular release (6). The mPSC rate returned to baseline as the temperature relaxed to prestimulus levels.
2. Temperature-sensitive ion channels in the plasma membrane (see the Supporting Material) were activated by a tonic-accumulated temperature increase, generated using pulse trains summating to

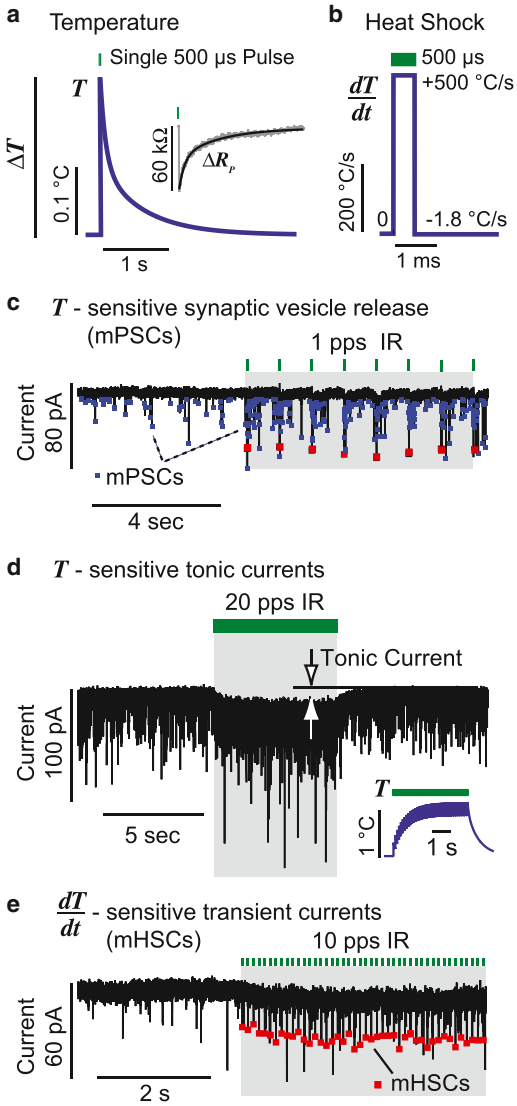

FIGURE 1 (*a*) Temperature was monitored ~400 μm in front of the IR optical fiber by measuring the resistance of a calibrated glass pipette, and is shown after calibration as the double-exponential curve. (*Inset*) Example of raw resistance data. (*b*) *dT/dt* approached 500°C s^{-1} during a 500-μs IR pulse and became slightly negative (−1.8°C s^{-1}) during thermal relaxation. Voltage-clamp recordings from the NMJ revealed three distinct types of thermally evoked currents: (*c*) an increase in the rate of presynaptic vesicle release (mPSCs) after each IR pulse that recovered with thermal relaxation of the tissue for IR stimuli at 1 pulse per s (pps); (*d*) an excitatory conduction current that had a slow onset and tracked the buildup of accumulated temperature (*inset*) caused by 20 pps IR; and (*e*) a miniature heat shock current (mHSC), sensitive to *dT/dt*, that occurred during each IR laser pulse (present in panels *c–e*, indicated by *red squares* in *c* and *e*). To see this figure in color, go online.

$$T_{\mathrm{TONIC}} \sim \Delta T\left\{\left(1-\phi e^{-\Delta t/\tau_1} - (1-\phi)e^{-\Delta t/\tau_2}\right)^{-1} - 1/2\right\},$$

where $1/\Delta t$ is the pulse rate, pps.

3. Each IR pulse evoked an inward miniature heat shock current (mHSC) (Fig. 1 *e*) that initiated during the heat

shock while the laser was on ($dT/dt > 0$) and rapidly decayed when the laser was off ($dT/dt \sim 0$).

The third photothermal effect, the dT/dt-sensitive mHSC, is the topic of this report.

Without exception, each IR pulse evoked an excitatory mHSC with onset coinciding with the optical stimulus and decay beginning with cessation of the optical stimulus. For a 500-μs pulse, mHSCs resembled mPSCs, thus leading us to investigate whether the currents might have origins in IR gating of postsynaptic receptors. To rule this out we recorded mHSCs in mutant *C. elegans* that did not express one or more of the established postsynaptic receptors: a γ-aminobutyric acid receptor, a levamisole-sensitive acetylcholine receptor (ACh_R), or a nicotine-sensitive ACh_R. Results in Fig. 2, *a* and *b*, show mHSCs were unchanged in these mutants. This is most clearly illustrated by stimulus-triggered averages (Fig. 2 *b*), showing that the mHSC waveforms were nearly identical in all cases. The small ringing and differences in recovery to baseline are likely due to limitations of the voltage-clamp and are unlikely to reflect actual differences in the mHSCs (see the Supporting Material).

To further confirm mHSCs were independent of major ionic conduction currents, we also recorded mHSCs in the absence of extracellular Ca^{2+}, Na^+, and K^+, and observed mHSCs in all cases (Fig. 2 *c*). mHSCs also persisted (Fig. 2 *d*) in the presence of ruthenium red (40 μMm; Tocris Bioscience, Bristol, UK) and a form of benzothiazepine (20 μM CGP37157; Tocris Bioscience, Bristol, UK), compounds known to interfere with IR-evoked intracellular Ca^{2+} transients presumably by blocking intracellular calcium channels (2). In addition, the onset latency of the mHSCs was zero (immeasurably small), which ruled out IR-evoked molecular signaling as a potential trigger for the mHSCs.

To determine the dependence of the mHSC on the temperature rise per pulse (ΔT) versus the time rate of rise (dT/dt), we varied the IR pulse-width inversely with the laser power to achieve stimuli of constant temperature rise ΔT (0.25°C) but variable dT/dt (300–1500 μs pulses, 667–133°C s^{-1}). Raw mHSCs evoked by a 500-μs pulse are shown for one cell in Fig. 3 *a*, and stimulus-triggered averages for 17 cells are shown in Fig. 3 *b*. The stimulus-triggered average removes any slowly developing tonic PSC that might have been present (e.g., Fig. 1 *c*) and reveals only the pulse-by-pulse IR evoked current. The single pulse-evoked mHSC increased amplitude exponentially toward a plateau, and decayed with the same time constant after cessation of the IR stimulus. The rate of temperature rise dT/dt was constant during these stimuli and therefore cannot explain the exponential rise or fall. Furthermore, the thermal relaxation time was more than two-orders-of-magnitude slower than the mHSC time constant, ruling out the possibility that part of the exponential rise or decay was due to thermal diffusion.

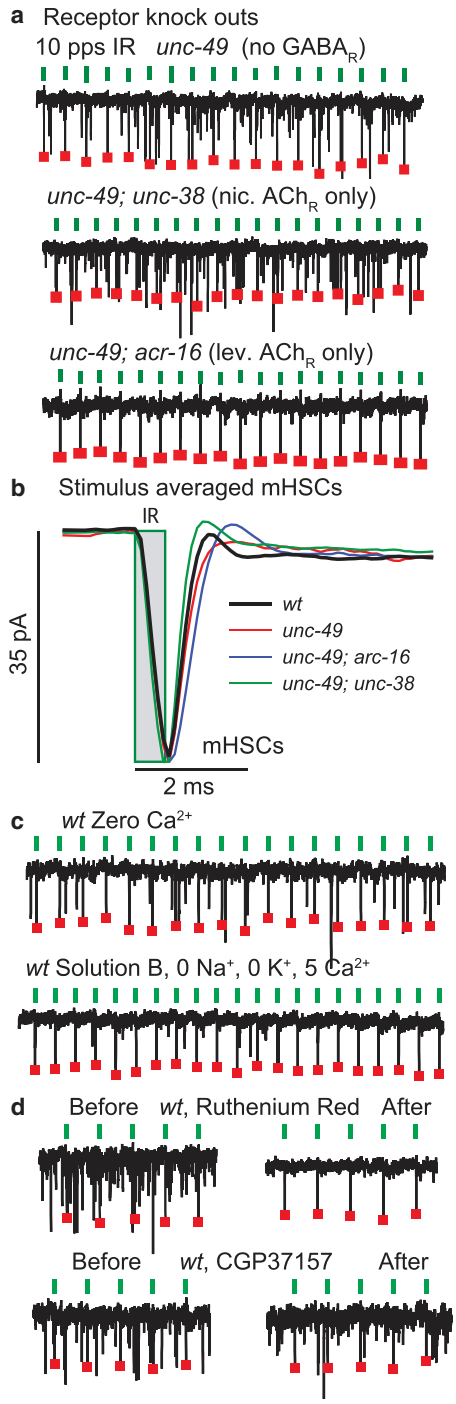

FIGURE 2 (*a*) Whole-cell voltage-clamp recordings at −60 mV in WT and mutant *C. elegans* (*unc-49, unc-49;unc-38, unc-49;acr-16*) revealed mHSCs to be completely independent of NMJ postsynaptic receptor expression ($n = 14$; γ-aminobutyric acid receptor, nicotine-sensitive ACh_R, and levamisole-sensitive ACh_R). (*b*) IR pulses triggered nearly identical photothermal currents in WT and the three receptor mutants. (*c*) mHSCs persisted in zero extracellular Ca^{2+} and persisted after removing key ionic charge carriers from the bath. (*d*) mHSCs also persisted in the presence of compounds shown previously to block heat pulse-evoked intracellular Ca^{2+} transients. To see this figure in color, go online.

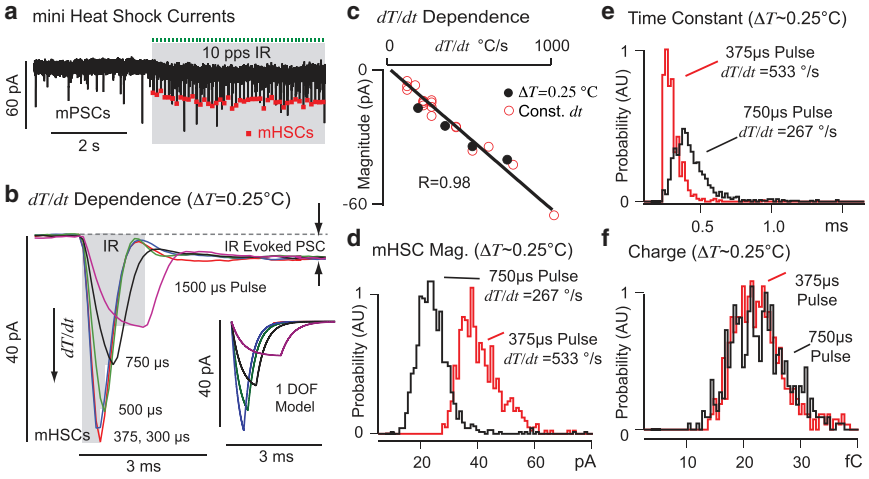

FIGURE 3 (*a*) Cells responded to each IR pulse with a single mHSC ($n = 79$ WT; IR 500 μs, $\Delta T \sim 0.25°C$). (*b*) Stimulus-triggered averages provided the amplitude and time course of mHSCs ($n = 17$; 50 mHSCs/cell). Varying the laser power inversely with the pulse-width (*dt*) delivered constant energy ($E = 1.5$ mJ) and constant temperature increase per pulse, thus revealing dependence of the mHSC amplitude and kinetics on *dT/dt*. In contrast, the long latency, IR-evoked PSC (*b*, *arrows*) was independent of *dT/dt*, providing the temperature-rise ΔT was the same for each stimulus. A model describing temperature dependence of the membrane electrical double layer quantifies the mHSCs (*b*, *inset*, Eqs. 1–3). (*c*) The magnitude of the mHSC increased linearly with the heat shock when *dT/dt* was delivered with 1), constant ΔT delivered by inversely varying laser power and *dt*, or 2), variable temperature rise (ΔT) delivered using a sequence of laser powers at constant pulse width (*dt*). (*d–f*) Histograms comparing mHSCs for a 750-μs pulse (267°C s^{-1}) versus a 375-μs pulse (533°C s^{-1}) with the IR power adjusted to deliver identical ΔT for all pulses reveal significant increases in (*d*) magnitude and (*e*) speed with shorter pulses, but no change in (*f*) net charge displacement ($n = 17$, 50 mHSCs/cell). Results show the charge displacement depends on ΔT and, concomitantly, the current depends on *dT/dt*. To see this figure in color, go online.

Rather than reflecting temperature kinetics, the recorded time constants reflect the time constant of the voltage-clamp (~150 μs) plus the time required for the electrical current to develop. Time constants in this data exceeded the voltage-clamp time constant, and were not corrected for the finite speed of the clamp (see the Supporting Material). For the short pulses studied, the mHSC amplitude increased linearly with *dT/dt* (Fig. 3, *b–d*). Linear dependence on *dT/dt* held for pulses of constant temperature-rise ($\Delta T = 0.25°C$) with the rate adjusted by varying the laser power inversely with pulse-width (Fig. 3 *c*, *solid symbols*), and for pulses of variable temperature-rise by varying the laser power with constant pulse-width (Fig. 3 *c*, *open symbols*). The onset and decay time constants decreased with *dT/dt* (Fig. 3 *e*). Probability histograms accumulated for 17 cells show clear shifts in the mean amplitude and speed for different heat deposition rates (Fig. 3, *d–e*, e.g., *dT/dt* =267 vs. 533°C s^{-1}). In contrast, the net charge displacement, obtained by the time integral of the mHSC component of the current (after subtracting long latency IR-evoked PSC discussed below), was completely independent of the rate *dT/dt* and depended only on the temperature rise ΔT. The mean charge displacement for a 0.25°C temperature rise was ~23 ± 6.4 fC. These results prove the mHSC arises from a temperature-dependent electrical charge displacement, and hence is a capacitive photothermal current.

In addition to the capacitive photothermal mHSC, stimulus-averaged currents revealed a long latency, IR-evoked, postsynaptic current (PSC) (Fig. 3 *b*, *arrows*) that was sensitive to the temperature rise but completely insensitive to the rapid rate of change during the IR pulse. This is shown in Fig. 3 *b* by convergence of all IR-evoked PSCs for latencies >4 ms irrespective of the size of *dT/dt*. Results demonstrate that the IR-evoked PSC was driven by the temperature rise (ΔT), independent of the rate of change during the short IR pulse. This ΔT-sensitive component of the current arises from the temperature-driven increase in the rate of presynaptic vesicular release illustrated in Fig. 1 *c*. Stimulus-triggered averaging smoothes the IR-evoked mPSCs to reveal a net excitatory current arising from increased presynaptic release rate. For a 0.25°C temperature rise, the stimulus-averaged IR-evoked PSC reached a peak of −4 pA at a latency of ~5 ms after the onset of the stimulus, and decayed to zero after relaxation of the temperature. Although we did not record from the presynaptic neuron, these results show that the IR-evoked increase in synaptic vesicle release was independent of *dT/dt* and therefore likely to be independent of the capacitive photothermal effect in the presynaptic neuron. The key variable evoking presynaptic vesicular release was likely temperature itself.

Fig. 4 reports voltage sensitivity of the capacitive photothermal mHSC. The mHSC reversal potential was close to −13 mV (Fig. 4, *a* and *b*), and distinct from the zero current potential of −30 mV in these cells. Voltage sensitivity was almost unchanged in zero extracellular Ca^{2+}. Responses also persisted with removal of Na^+ and K^+ from the bath, and with Cs, TEA, and 4-AP in the pipette (Fig. 4 *b*). Therefore, mHSCs were independent of major membrane conduction currents, yet exhibited a reversal potential and voltage sensitivity dependent upon ionic composition of the bath.

It was shown previously in model membranes and cell lines that pulsed photothermal stimulation evokes a capacitive current arising from temperature dependence of the plasma membrane electrochemical double layer (17). The double layer is classically described as consisting of the diffuse Gouy-Chapman (18,19) layer and the relatively immobile Stern layer (i.e., Gouy-Chapman-Stern (GCS) model) (20), and is illustrated schematically in Fig. 5. The

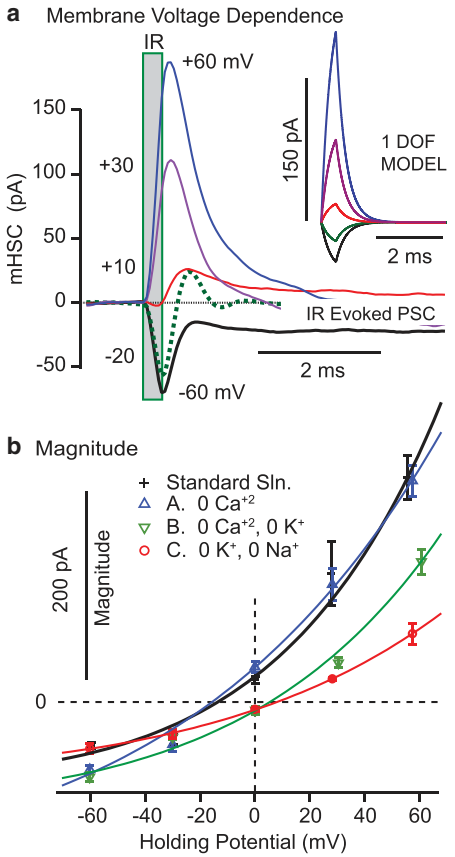

FIGURE 4 mHSC voltage sensitivity. (*a*) Stimulus-triggered average currents revealed mHSCs reversal near −13 mV in standard media. (*b*) Amplitude of the mHSC versus holding potential in various solutions: + standard, *A* (0 Ca^{+2}), *B* (0 Ca^{+2}, 0 K^+), and *C* (0 K^+, 0 Na^+). Error bars signify standard error. mHSC kinetics and voltage dependence is captured by a 1-DOF model of temperature-dependent membrane double layer (*a*, *inset*; *b*, *solid curves*). To see this figure in color, go online.

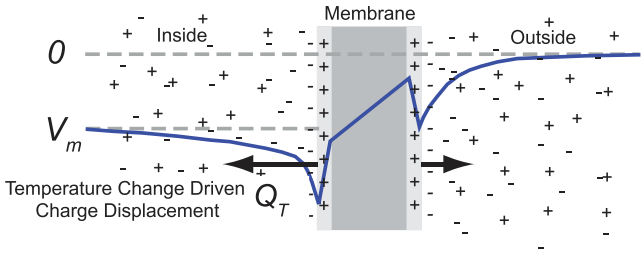

FIGURE 5 Schematic of the plasma membrane electrochemical double layer. Absorption of IR light by water causes a rapid increase in temperature that displaces ions within the double layer asymmetrically on both sides of the membrane. This leads to a net charge displacement $Q_T{}^{\infty}$ driven by temperature, and thereby a net current driven by the rate of change of temperature. To see this figure in color, go online.

double-layer electric field and the spatial distribution of ions are temperature-dependent, so changing temperature displaces net charge. Using the chain rule, the photothermal double-layer current (mHSC) is given by the temperature derivative of the net double-layer charge $Q_T{}^{\infty}$ times the time rate of change of temperature T,

$$I^{\infty} = \frac{dQ_T^{\infty}}{dT}\frac{dT}{dt}, \tag{1}$$

where the ∞ superscript denotes equilibrium (steady state). The double-layer is composed of multiple interacting ions, differing on the two sides of the membrane. Temperature increases stretch the intra- and extracellular double layers to differing extents and thereby evokes a net charge displacement. The net charge $Q_T{}^{\infty}$ can be determined from first-principles based on the ionic compositions, dielectric constants, and membrane potential (17,22). The temperature derivative $dQ_T{}^{\infty}/dT$ from the GCS theory can be written in the following form (see the Supporting Material):

$$I^{\infty} = \sum_{j=1}^{J} I_j^{\infty} = \frac{dT}{dt}\frac{dQ_T^{\infty}}{dT}$$
$$= \frac{dT}{dt}\left(\sum_{j=1}^{J}\alpha_j\left[\frac{1+(V-\phi_j)/\beta_j}{\exp\{-(V-\phi_j)/\beta_j\}}-1\right]\right). \tag{2}$$

Here the sum is over all intracellular (odd j) and extracellular (even j) ions; $\alpha_j = \varepsilon R c^{i}{}_j$ for intracellular ions; $\alpha_j = \varepsilon R c^{\circ}{}_j$ for extracellular ions and provides the charge displacement per degrees-centigrade change; $\beta_j = RT/Fz_j$ (V) is the Boltzmann voltage sensitivity; $\phi_j(V)$ is the ζ-potential on the intra- or extracellular side of the membrane; and V is the membrane potential for intracellular ions, which is 0 for extracellular ions; ε = electrical permittivity of media; R = ideal gas constant; T = absolute temperature; F = Faraday's constant; and z = valence. In this full form, the sum is over J intracellular and extracellular ions.

The Poisson equation enforces space charge neutrality and couples ion movements together, with kinetics dictated by electrochemical diffusion within the diffuse layer and kinetics of the relatively immobile Stern layer. The photothermal capacitive current (mHSC, Figs. 4 and 5) recorded in these experiments reflects this net displacement of all ions together. The data show the net current was dominated by a single capacitive reversal potential (Fig. 5), suggesting use of an empirical model where groups of ions are lumped together. To take advantage of this, we introduce a lumped model where Eq. 2 governs the steady-state current, but each term in the sum represents a group of ions moving together rather than an individual ion. With this, α_j ($pC^{\circ}C^{-1}$) becomes the gain, β_j (mV) becomes the voltage sensitivity, and ϕ_j (mV) becomes the capacitive reversal potential of the jth group of ions. We further simplified the model to one degree of freedom (1-DOF, $J = 1$), and numerically optimized the parameters (α_1, β_1, ϕ_1) to fit the equilibrium currents in Fig. 4 *b* (parameters summarized in Table 1). This collapses contributions from multiple ions on both sides of the membrane into one simple expression with three independent parameters. It is important to note

TABLE 1 DOF model parameters

Solution	α_1 pC/°C	β_1 mV	ϕ_1 mV
Standard	0.153	80.9	−12.9
A, 0 Ca^{+2}	0.321	139.4	−15.2
B, 0 Ca^{+2}, K^+	0.198	103.4	5.87
C, 0 Ca^{+2}, K^+, Na^+	0.143	123.1	8.96

that the steady-state current I^∞ is highly sensitive to dT/dt (directly proportional), but depends only weakly on temperature itself (through linear temperature dependence of β on absolute T, $Q_{10} \approx 1$).

Equation 2 describes the steady-state current once equilibrium has been reached and does not address the time required to develop the current as dictated by kinetics of electrochemical diffusion in interactions within the double layer. This is a nonlinear process dependent on voltage and the specific ionic milieu. Our results revealed nearly exponential kinetics of the net current (Fig. 3 *b*), with time constants varying between stimulus parameters. For simplicity, we modeled the transient using first-order kinetics with the steady-state current given by the 1-DOF version of Eq. 2 and the instantaneous current governed by

$$\frac{dI_j}{dt} + \frac{I_j}{\tau_j} = \frac{I_j^\infty}{\tau_j}, \tag{3}$$

where τ_j is a stimulus-dependent time constant (Fig. 3, *b* and *e*). The time constant ($j = 1$) was determined empirically from results in Fig. 4 *a* using

$$\tau_1 = 150 + 28 \Big/ \sqrt{dT/dt} \ \ \mu s.$$

The 150-μs offset is due to the limited speed of the voltage-clamp, which filtered all records to a time constant >150 μs (see the Supporting Material). The square-root dependence on the rate likely arises from thermally driven diffusion. Mathematical similarity of the one-dimensional diffusion equation requires the nondimensional similarity group

$$\tilde{x} \Big/ \sqrt{4D\tilde{t}}$$

to be of order one, where $\tilde{x}$ is the characteristic diffusion distance and $\tilde{t}$ is the characteristic time. The characteristic distance $\tilde{x}$ would be expected to be proportional to the charge displacement, which was constant for results reported in Fig. 3, *d–f*. For a linear increase in temperature over time $\tilde{t}$ the diffusion coefficient would have the form

$$D = D_0 + r\tilde{t},$$

where r is the time rate of change of the diffusion coefficient and is proportional to dT/dt.

Assuming the similarity group is order one, and expanding for large r in a Taylor series, provides

$$\tilde{t} = \tilde{x} \Big/ \sqrt{4r}.$$

The dependence on $1/\sqrt{r}$ indicates diffusion is likely the origin of the inverse square-root in our empirical formula for the time constant τ. In general, the characteristic charge displacement would scale with absolute temperature (see Eqs. S1 and S2 in the Supporting Material), thus suggesting the time constant τ would also scale with absolute temperature, but this expected temperature dependence was overwhelmed by rate dependence by more than two orders of magnitude in these experiments.

Predictions of this model are shown as insets in Fig. 3 *b* and Fig. 4 *a*, and by the solid curves in Fig. 4 *b*. Note, at −60 mV hold, the model predicts a large inward mHSC during heating and a much smaller outward mHSC during thermal relaxation. In this model, and from previous data in membranes (17), the photothermal capacitive current is thermodynamically conservative and integrates to zero over the full thermal transient. Because the heating time was more than two-orders-of-magnitude faster than thermal relaxation time, the inward component was large in amplitude whereas the outward component was small and not visible by eye in the figures. The current is thermodynamically conservative and capacitive because the net charge $Q_T{}^\infty$ depends only on temperature T. Once the temperature relaxes back to the prestimulus level the charge also returns to the prestimulus level.

It should be noted the model only addresses the dT/dt-dependent photothermal current (the mHSC) and does not address T-sensitive currents such as the IR-evoked PSC (Fig. 3 *b* and Fig. 1 *b*) or slowly developing membrane ionic currents (Fig. 1 *c*, and see Fig. S1 and Fig. S2 in the Supporting Material). Also, the 1-DOF model has a single capacitive reversal potential, so it cannot capture the multicomponent reversal and time constants associated with multiple ionic degrees of freedom present in the data (e.g., Fig. 3 *a*, *dotted curve* at −30 mV has at least two reversals of differing time constants, suggesting $J > 1$). Even with the 1-DOF simplification, the model captures major features of this mHSC data.

DISCUSSION

Our results quantify the magnitude and time course of capacitive photothermal membrane currents evoked in vivo using pulsed IR heating of water. The net charge displacement for a single IR pulse was a function of the temperature-rise ΔT, and was independent of the rate of rise over the full range tested (Fig. 3 *f*). As a result, the mHSC increased in proportion to the magnitude of dT/dt (Fig. 3 *c*). During IR optical stimulation, dT/dt was ~500°C s^{-1} and evoked a brief inward mHSC of ~35 pA. This generated ~0.25°C temperature-rise and injected ~23 fC of depolarizing charge. Under physiological conditions, for IR pulses

shorter than the cell membrane time constant, the whole-cell depolarization caused by this change injection would be

$$\Delta V \approx Q_T^{\infty} / C_m,$$

where C_m is the whole-cell membrane capacitance. Using the average capacitance measured in this study of 26 pF gives a membrane depolarization of ~880 μV per pulse, comparable to that caused by a single mPSC. This level of depolarization would be sufficient to trigger action potentials in highly sensitive neurons, but would fail in many neurons. Although the presence of capacitive photothermal membrane currents is likely universal, its relatively small size might limit efficacy as an excitatory stimulus to only the most voltage-sensitive cells.

It is important to note that the temperature-driven charge displacement $Q_T{}^{\infty}$ and the cell membrane capacitance C_m both scale with the surface area of the membrane and, therefore, depolarization should be independent of cell size, providing the heat shock is applied uniformly over the whole cell. If the heat shock were applied only to a fraction of the membrane, depolarization would reduce proportionally. Based on this data for a temperature-rise of 0.25°C, a charge displacement of 23 fC (Fig. 3 *f*, at −60 mV hold), a whole-cell capacitance of 26 pF, and a membrane specific capacitance of ~1 μF cm^{-2} (23), we estimate the specific charge displacement per unit membrane area and temperature-rise as

$$q^* \approx 3.5 \text{ nC} - \text{cm}^{-2} - {}^{\circ}\text{C}^{-1}.$$

Based on GCS theory, the specific numeral value of q^* would be expected to change somewhat in other cells with ionic composition and membrane potential. With this, the capacitive photothermal depolarization evoked by a single brief IR pulse can be estimated using

$$\Delta V \approx \left(\frac{q^* A}{C_m}\right) \frac{dT}{dt}, \tag{4}$$

where A is the membrane area exposed to the IR laser pulse. It is also important to note that the photothermal mHSC is a capacitive current that integrates to zero net charge over the full time course of the thermal transient. The fact that the positive heat shock is so short relative to negative relaxation makes the mHSC excitatory and resemble an inward conduction current.

SUPPORTING MATERIAL

Voltage-Clamp Speed, Temperature-Dependent Series Resistance, Temperature-Dependent Electrochemical Double Layer, Temperature vs. Heat Shock, Temperature-Dependent Ionic Conductance, four equations, two figures, and References (24,25), are available at http://www.biophysj.org/biophysj/supplemental/S0006-3495(14)00277-X.

We thank the Thomas and Horvitz labs for strains. Other strains were obtained from the Caenorhabditis Genetics Center.

Support was provided by National Institutes of Health grant No. R01-DC011481 (to R.D.R.), National Science Foundation grant No. DGE-0903715 (to M.J.F.), and National Institutes of Health grant No. R01-NS034307 and a Howard Hughes Medical Institute grant (to E.M.J.).

REFERENCES

1. Tseeb, V., M. Suzuki, …, S. Ishiwata. 2009. Highly thermosensitive Ca dynamics in a HeLa cell through IP_3 receptors. *HFSP J.* 3:117–123.
2. Dittami, G. M., S. M. Rajguru, …, R. D. Rabbitt. 2011. Intracellular calcium transients evoked by pulsed infrared radiation in neonatal cardiomyocytes. *J. Physiol.* 589:1295–1306.
3. Wells, J., C. Kao, …, A. Mahadevan-Jansen. 2005. Optical stimulation of neural tissue in vivo. *Opt. Lett.* 30:504–506.
4. Wells, J., P. Konrad, …, A. Mahadevan-Jansen. 2007. Pulsed laser versus electrical energy for peripheral nerve stimulation. *J. Neurosci. Methods.* 163:326–337.
5. Richter, C. P., S. M. Rajguru, …, J. T. Walsh. 2011. Spread of cochlear excitation during stimulation with pulsed infrared radiation: inferior colliculus measurements. *J. Neural Eng.* 8:056006.
6. Rajguru, S. M., C. P. Richter, …, R. D. Rabbitt. 2011. Infrared photostimulation of the crista ampullaris. *J. Physiol.* 589:1283–1294.
7. Bec, J. M., E. S. Albert, …, M. Dumas. 2012. Characteristics of laser stimulation by near infrared pulses of retinal and vestibular primary neurons. *Lasers Surg. Med.* 44:736–745.
8. Jenkins, M. W., A. R. Duke, …, A. M. Rollins. 2010. Optical pacing of the embryonic heart. *Nat. Photonics.* 4:623–626.
9. Smith, N. I., Y. Kumamoto, …, S. Kawata. 2008. A femtosecond laser pacemaker for heart muscle cells. *Opt. Express.* 16:8604–8616.
10. Wells, J., C. Kao, …, E. D. Jansen. 2007. Biophysical mechanisms of transient optical stimulation of peripheral nerve. *Biophys. J.* 93:2567–2580.
11. Norton, B., and M. Bowler. 2013. Green's function representation of laser induced thermal dynamics and determination of thermal criteria for optically induced neural activation. *Proc. SPIE.* 8579:Optical Interactions with Tissue and Cells XXIV, 857908 (February 15, 2013); http://dx.doi.org/10.1117/12.2007059.
12. Izzo, A. D., J. T. Walsh, Jr., …, C. P. Richter. 2008. Laser stimulation of auditory neurons: effect of shorter pulse duration and penetration depth. *Biophys. J.* 94:3159–3166.
13. Albert, E. S., J. M. Bec, …, C. Chabbert. 2012. TRPV4 channels mediate the infrared laser-evoked response in sensory neurons. *J. Neurophysiol.* 107:3227–3234.
14. Liljemalm, R., T. Nyberg, and H. von Holst. 2013. Heating during infrared neural stimulation. *Lasers Surg. Med.* 45:469–481.
15. Schultz, M., P. Baumhoff, …, A. Kral. 2012. Nanosecond laser pulse stimulation of the inner ear—a wavelength study. *Biomed. Opt. Express.* 3:3332–3345.
16. Wang, L. V., and H.-i. Wu. 2007. Biomedical Optics: Principles and Imaging. Wiley-Interscience, Hoboken, N.J..
17. Shapiro, M. G., K. Homma, …, F. Bezanilla. 2012. Infrared light excites cells by changing their electrical capacitance. *Nat. Commun.* 3:736.
18. Chapman, D. 1913. A contribution to the theory of electrocapillarity. *Philos. Mag.* 25:475–481.
19. Gouy, G. 1909. In the constitution of the electric charge on the surface of an electrolyte [Sur la constitution de la charge électrique à la surface d'un électrolyte]. *Compt. Rend.* 149:654–657.
20. Stern, O. 1924. For the theory of the electrolytic double layer [Zur theorie der elektrolytischen doppelschicht]. *Z. Elektrochem.* 30:508–516.
21. Liu, Q., G. Hollopeter, and E. M. Jorgensen. 2009. Graded synaptic transmission at the *Caenorhabditis elegans* neuromuscular junction. *Proc. Natl. Acad. Sci. USA.* 106:10823–10828.

22. Genet, S., R. Costalat, and J. Burger. 2000. A few comments on electrostatic interactions in cell physiology. *Acta Biotheor.* 48: 273–287.

23. Gentet, L. J., G. J. Stuart, and J. D. Clements. 2000. Direct measurement of specific membrane capacitance in neurons. *Biophys. J.* 79:314–320.

24. Santi, C. M., A. Yuan, …, L. Salkoff. 2003. Dissection of K^+ currents in Caenorhabditis elegans muscle cells by genetics and RNA interference. *Proc. Natl. Acad. Sci. USA.* 100:14391–14396.

25. Yuan, A., C. M. Santi, …, L. Salkoff. 2003. The sodium-activated potassium channel is encoded by a member of the Slo gene family. *Neuron.* 37:765–773.

Supporting Material

Exciting Cell Membranes with a Blustering Heat Shock

Liu Q, Frerck MJ, Holman HA, Jorgensen EM, Rabbitt RD

Voltage Clamp Speed. All experiments were performed using single electrode voltage clamp with the resting capacitive transients fully compensated and series resistance compensated 50%. Under these conditions the electrode current I_{EC} is related to the total membrane conduction current I_m and the thermally modulated capacitive charge displacement Q_T by $\tau_{VC}\frac{dI_{EC}}{dt} + I_{EC} = I_m + \frac{dQ_T}{dt}$, where τ_{VC} is the voltage clamp time constant. The voltage clamp time constant is approximated by the uncompensated portion of the electrode resistance multiplied by the resting membrane capacitance $\tau_{VC} \approx R_E C_m$. Recordings were not corrected for τ_{VC} and therefore currents with time constants faster than ~150μs were not resolved. All data in the present report contain this artificial low-pass filter.

Temperature Dependent Series Resistance. Patch pipettes used in the present experiments had nominal resistance of ~5MΩ. The conductance of physiological salt solutions is temperature dependent and as a result the series resistance modulated with temperature. The relationship between pipette conductance G and temperature is linear on an Arrhenius scale and given by $G = Ae^{-E_A/RT}$ (e.g. $A \approx e^{11.9}$, with energy $E_A \approx 3.4 \times 10^4$). For a single 500μs, 1.5mJ IR pulse the patch pipette reduced series resistance by ~1%. Hence, we did not correct for temperature dependent series resistance in single pulse results reported in the parent manuscript. Modulation of series resistance becomes larger for pulse trains, so results shown in Fig. S2 were corrected for this temperature dependent series resistance change.

Temperature Dependent Electrochemical Double Layer.

To explicitly describe the equilibrium current during the heat shock we followed the approach of Shapiro et al. (1) and applied the classical Gouy-Chapman-Stern (GCS) theory (2-4). From GCS, the double layer charge on the extracellular and intracellular sides of the membrane are (5),

$$\left(Q_0^{\infty}\right)^2 = \left(\sigma_o + \frac{\varepsilon_m}{\delta}\left(\zeta_i - \zeta_o\right)\right)^2 = 2\varepsilon_s RT\sum_{k=1}^{K} c_k^0\left(\exp\left(\frac{-z_k F\zeta_o}{RT}\right)-1\right), \quad \text{(s1)}$$

$$\left(Q_i^{\infty}\right)^2 = \left(\sigma_i - \frac{\varepsilon_m}{\delta}\left(\zeta_i - \zeta_o\right)\right)^2 = 2\varepsilon_s RT\sum_{k=1}^{K} c_k^i\left(\exp\left(\frac{-z_k F\left(\zeta_i - V_m\right)}{RT}\right)-1\right) \quad \text{(s2)}$$

where "o" and "i" correspond to extracellular and intracellular. ε_m and ε_s are the electrical permittivity of the membrane and physiological ionic media, δ is the thickness of the membrane, σ is the membrane intrinsic charge, R is the ideal gas constant, T is temperature, F is Faraday's constant, c_k is the concentration of the k^s ion, z_k is the valence, V_m is the membrane potential, ϕ_i is the voltage on the inside surface of the membrane and ϕ_o is the voltage on the outside surface of the membrane. For small charge displacements, the temperature derivative gives

$$\frac{dQ_T^{\infty}}{dt} \approx \varepsilon R\sum_{k=1}^{K}\left\{c_k^i\left(\frac{1+\left(V_m-\zeta_i\right)Fz_k/RT}{Exp\left(-\left(V_m-\zeta_i\right)Fz_k/RT\right)}-1\right)-c_k^o\left(\frac{1-\zeta_o Fz_k/RT}{Exp\left(\zeta_o Fz_k/RT\right)}-1\right)\right\}, \quad \text{(s3)}$$

and can be rewritten as

$$\frac{dQ_T^{\infty}}{dt} = \sum_{j=1}^{J}\alpha_j\left[\frac{1+\left(V-\zeta_j\right)/\beta_j}{exp\left(-\left(V-\zeta_j\right)/\beta_j\right)}-1\right] \quad \text{(s4)}$$

where $\beta_j = RT / Fz_j$ and the sum is over all intracellular (odd j) and extracellular ions (even j). $\alpha_j = \varepsilon R c_j^i$ for intracellular ions and $\alpha_j = -\varepsilon R c_k^o$ for extracellular ions. V is the membrane potential for intracellular ions and is zero for extracellular ions. ζ_j is ζ_i for intracellular ions or ζ_o for extracellular ions.

Temperature vs. Heat Shock. IR evoked currents were categorized as one of two types: 1) heat shock sensitive (dT / dt sensitive) or 2) temperature sensitive (T sensitive). Fig. S1 shows both types of currents. A single IR pulse evoked a single dT / dt sensitive mHSC, a burst of mPSCs, and a T-sensitive inward PSC that slowly returned to baseline as the temperature relaxed (S1A). We used IR pulse trains to generate an accumulated temperature rise T_{TONIC} (S1B) (6) and to evoke a tonic PSC (S1C). The accumulated temperature is the result of the summation of thermal transients arising from individual pulses and occurs when pulses are presented at a rate faster than the thermal relaxation time (6). The T-sensitive PSC followed the accumulated temperature and increased magnitude to reach a tonic plateau. The magnitude of the tonic PSC increased with IR power (Energy/pulse times pulses per second, E*pps). The tonic PSC and the mHSC both scaled with the thermal energy delivered thus leading to a linear correlation between the tonic PSC and the mHSC amplitude as the energy per pulse was increased (S1D).

Temperature Dependent Ionic Conductance. Fig. S2 reports the contribution of SLO-2 to the temperature sensitive tonic current. When held at -60mV, cells in *wt* animals and *slo-2* mutants responded almost identically to ΔT with a tonic net inward current, or reduction of outward current (S2A,B). There were no differences between *wt* and *slo-2* in the mHSC or the short latency onset responses to IR, showing that SLO-2 does not contribute to heat shock dT / dt responses. When depolarized to +60mV, cells from *wt* animals exhibited a large delayed inward current (or reduction of outward current). This current built up slowly and did not directly follow the temperature rise. The delayed onset and buildup shows a signaling mechanism was involved and that the response was not a direct temperature effect on the channel. The delayed current was completely

abolished in the *slo-2* mutant (S2A,B). It has been shown previously that *C. elegans* SLO-2 is activated by intracellular Ca^{2+}/Cl^- (7, 8). Therefore it is likely that the SLO-2 current was a downstream consequence of thermal stimuli slowly altering intracellular Ca^{2+} and/or Cl^-. Although interesting, these events require a build up of temperature and are not germane to the focus of the parent manuscript, the capacitive photothermal current mHSC.

Supplement Figures

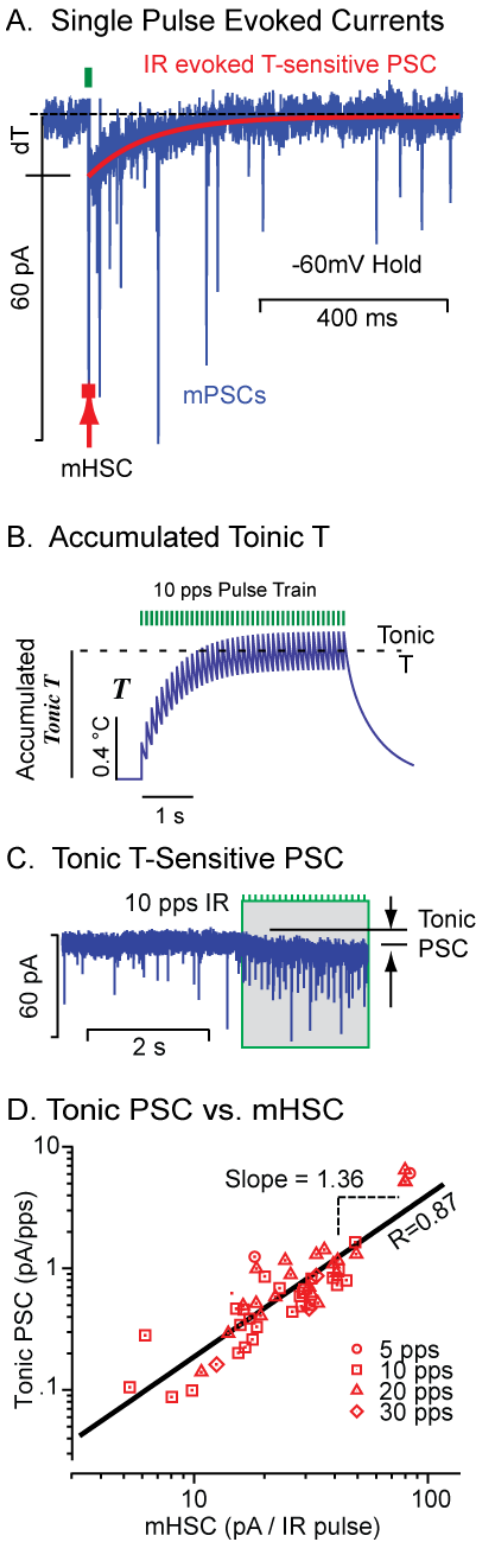

Fig. S1. A) Currents evoked by each IR pulse included a single mHSCs coincident with the pulse, mPSCs occurring after the pulse, and an IR evoked inward current that decayed with thermal relaxation. The T sensitive inward conductive PSC overwhelmed the small outward component of the dT/dt sensitive capacitive mHSC, both decaying in time with thermal relaxation. B) Temperature followed the time course detailed previously (6, 9). The increase during each pulse was linear in time and in the present work we approximated the relaxation using $T = \Delta T\left\{\phi e^{-t/\tau_1} + (1-\phi)e^{-t/\tau_2}\right\}$, where ΔT is the single pulse temperature rise. Using the single pulse as a Green's function, pulse train stimuli exceeding several seconds generated a plateau accumulated temperature rise of

$$T_{TONIC} = \Delta T\left\{\left(1-\phi e^{-\Delta t/\tau_1} - (1-\phi)e^{-\Delta t/\tau_2}\right)^{-1} - 1/2\right\},$$

where $1/\Delta t$ is the pulse repetition frequency (present experiments, $\tau_1 = 0.65$, $\tau_2 = 0.084$ and $\phi = 0.454$). C) T_{TONIC} evoked a tonic PSC. D) For IR stimuli of fixed pulse widths, but variable energy per pulse (variable dT/dt and temperature rise per pulse ΔT), the magnitude of the tonic PSC correlated linearly with the magnitude of dT/dt per pulse and the amplitude of the mHSC.

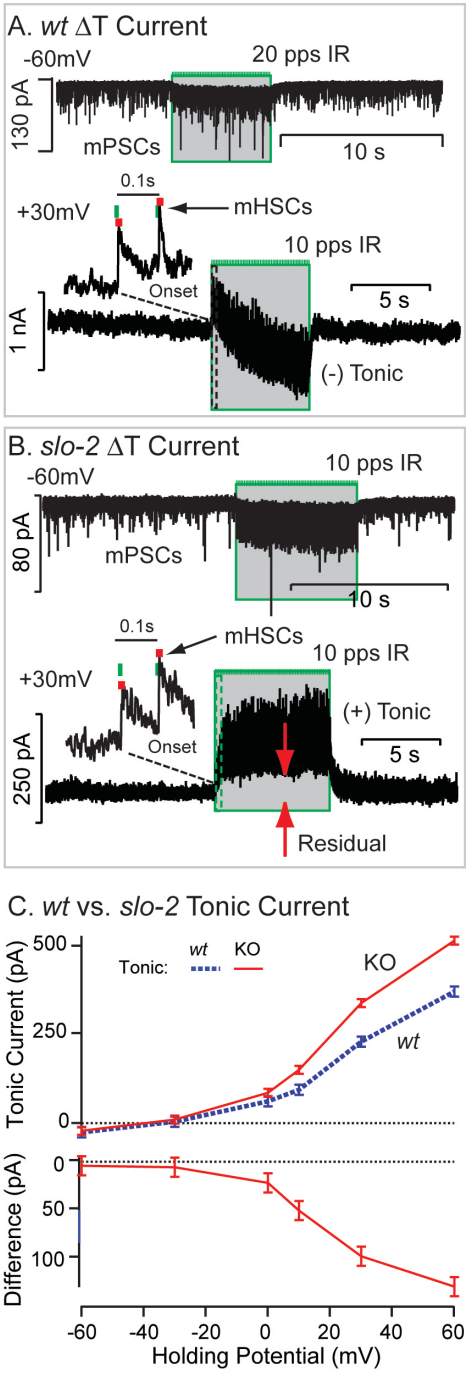

Fig. S2. The most substantial T-sensitive tonic PSC was eliminated in a SLO-2 KO. A) Depolarization reveals build up of a tonic PSC due to accumulated temperature $T_{TONIC} \approx 0.8\,^{\circ}\mathrm{C}$ in *wt* animals. This current is superimposed on top of the heat shock evoked mHSCs. B) The delayed tonic current was eliminated in SLO-2 KO. There was no change in the heat shock response (mHSCs). There was a "residual" ΔT dependent current that persisted in *slo-2*. C) Tonic currents are shown as functions of holding potential after compensating for temperature dependence of the pipette resistance using $I_{corrected} = \left(R_p / R_{corrected}\right) * I$. Subtraction shows a substantial change in current in the *slo-2* mutant.

Supplement Citations

1. Shapiro, M. G., K. Homma, S. Villarreal, C. P. Richter, and F. Bezanilla. 2012. Infrared light excites cells by changing their electrical capacitance. Nat Commun 3:736.
2. Chapman, D. 1913. A Contribution to the Theory of Electrocapillarity. Philos. Mag. 25:475-481.
3. Gouy, G. 1909. Sur la constitution de la charge électrique à la surface d'un électrolyte. Compt. Rend. 149:654-657.
4. Stern, O. 1924. Zur Theorie der Elektrolytischen Doppelschicht. Z. Elektrochem. 30:508-516.
5. Genet, S., R. Costalat, and J. Burger. 2000. A few comments on electrostatic interactions in cell physiology. Acta Biotheoretica 48:273-287.
6. Norton, B., and M. Bowler. 2013. Green's function representation of laser induced thermal dynamics and determination of thermal criteria for optically induced neural activation. SPIE:8579.
7. Santi, C. M., A. Yuan, G. Fawcett, Z. W. Wang, A. Butler, M. L. Nonet, A. Wei, P. Rojas, and L. Salkoff. 2003. Dissection of K+ currents in Caenorhabditis elegans muscle cells by genetics and RNA interference. Proc Natl Acad Sci U S A 100:14391-14396.
8. Yuan, A., C. M. Santi, A. Wei, Z. W. Wang, K. Pollak, M. Nonet, L. Kaczmarek, C. M. Crowder, and L. Salkoff. 2003. The sodium-activated potassium channel is encoded by a member of the Slo gene family. Neuron 37:765-773.
9. Liljemalm, R., T. Nyberg, and H. von Holst. 2013. Heating during infrared neural stimulation. Lasers Surg Med.